Macromolecules

ARTICLE

pubs.acs.org/Macromolecules

Effect of Block Copolymer Architecture on the Thermally Induced Swelling of Micelle-Containing Multilayer Thin Films

Wui Siew Tan,[†] Zhichen Zhu,[§] Svetlana A. Sukhishvili,[§] Michael F. Rubner,[*,†] and Robert E. Cohen[*,‡]

[†]Department of Materials Science and Engineering, Massachusetts Institute of Technology, 77 Massachusetts Avenue, Cambridge, Massachusetts 02139, United States

[§]Department of Chemistry, Chemical Biology and Biomedical Engineering, Stevens Institute of Technology, Hoboken, New Jersey 07030, United States

[‡]Department of Chemical Engineering, Massachusetts Institute of Technology, 77 Massachusetts Avenue, Cambridge, Massachusetts 02139, United States

Supporting Information

ABSTRACT: We investigate the effect of block copolymer (BCP) molecular weight and connectivity on the morphology and time−temperature dependent swelling of thin film hydrogels created through layer-by-layer (LbL) assembly of BCP micelles with poly(acrylic acid). BCPs of poly(*N*,*N*-dimethylaminoethyl methacrylate) (D) and poly(propylene oxide) (P), a P−D diblock, a long D−P−D triblock, and a short D−P−D triblock copolymer, were compared in terms of their temperature response in solution and within micelle−polyelectrolyte multilayers (mPEMs). The critical micellization concentration and micellization temperature of the BCPs in solution, as well as the swelling transition temperature, T_{stt}, of the mPEMs, decreased with increasing P block length. AFM imaging of dry mPEMs shows regular dimpled surface structures that arise from surface relaxation of micelles. When the mPEMs are cooled below T_{stt} in water, the thin ∼200 nm films can swell reversibly between 3 and 6 times their dry thicknesses within 2 min. The degree of swelling (τ = wet thickness/dry thickness) increases with undercooling ($\Delta T = T_{stt} - T$) and shows time dependencies related to ΔT and the constituent BCP connectivity. While the diblock films swell uncontrollably and lose integrity within 30 min at $\Delta T \geq 6$ °C, the triblock copolymer multilayers are able to sustain steady τ values (in the range of 4−10) under equivalent conditions. The differences in dynamic swelling behavior originating from BCP architecture have important implications in their utility as temperature responsive surfaces.

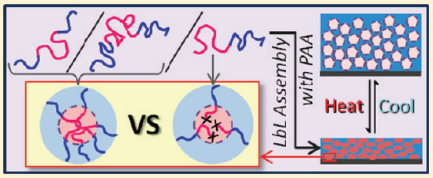

1. INTRODUCTION

Stimuli-triggered changes in the degree of swelling of thin hydrogel coatings allow active control of surface properties that include mechanical compliance,[1,2] solute permeability,[3] and chemical affinity.[4,5] Consequently, such coatings are sought after for applications in therapeutic delivery,[6,7] mechanical actuation,[8] molecular separations,[4] and sensing.[9] Controlling the mechanical properties of surfaces is also of critical importance at synthetic and biological interfaces as cell responses[10,11] and bacterial attachment[12] can be modulated by substrate compliance. Layer-by-layer (LbL) assembly is a facile conformal coating technique well suited for the creation of responsive thin film hydrogels. pH responsive LbL assemblies that exhibit large changes in swelling with pH variation have been created in the form of flat films,[13,14] capsules,[15,16] and within membrane pores,[17] with successful applications in controlled drug release[18] as well as membrane gating.[17] In contrast, there have been few reports of LbL assemblies able to exhibit large swelling transitions in response to temperature. Over the past few years, several efforts have been made to create temperature responsive multilayer thin films through the incorporation of temperature responsive polymers utilizing either hydrogen bonding[19] or electrostatic[20] LbL assembly. There have been demonstrations of temperature responsive LbL systems able to reversibly load and release small molecules[21−23] and therapeutics[24] as well as examples of systems that allow for temperature-triggered dissolution.[25,26] Attempts to create PEMs with large reversible swelling responses to temperature, however, have shown that polymers or copolymers that exhibit reversible temperature responses in solution, when incorporated into PEM films or capsules, showed limited temperature driven swelling changes that were irreversible.[20,27,28] While Jaber and Schlenoff have reported reversible temperature dependent hydration of multilayers at the molecular level,[29] and swelling ratios reversible between 1.1 (at 45 °C) and 1.65 (at 20 or 25 °C) were reported in studies by Zhu et al.[22] and Xu et al.,[23] these swelling degrees are small compared to typical hydrogels or the degree of swelling achievable in pH responsive LbL assemblies. In our previous work, LbL assembly of micelle forming block copolymers led to thin films that exhibit reversible swelling transitions of large scale, involving hydrated states with more than 400 vol % of water.[30] We found that the assembly pH and the anionic binding partner used for LbL assembly of a micelle forming, temperature responsive, A−B−A triblock copolymer were critical factors

Received: June 21, 2011
Revised: August 2, 2011
Published: September 08, 2011

that determined whether or not large temperature driven swelling could be observed.[30]

Micelle polyelectrolyte multilayers (mPEMs) were first reported in 2006 by groups interested in micelles as nanoparticulate structures for porosity introduction in optical applications.[31,32] It was also recognized that the core−shell structure of micelles formed by block copolymers (hydrophobic core surrounded by a hydrophilic corona) allowed creation of local hydrophobic environments within multilayers created from all aqueous solutions.[33,34] This proved useful for loading of hydrophobic functional compounds.[18,33−38] In fact, owing to advances in BCP synthesis, the chemical functionality carried within the micelle core forming block can be selected relatively independently of the hydrophilic corona forming block. As such, BCP micelles present opportunities for creating thin films of novel functionality not limited by chemistries required for water solubility and complementary bonding required for LbL film assembly. In our work, we use this capability to create electrostatically assembled mPEMs that are responsive to temperature.

In this study, we investigate the impact of BCP molecular weight and connectivity on the temperature-driven swelling behavior of LbL assembled thin film hydrogels. Three block copolymers of poly(*N*,*N*-dimethylaminoethyl methacrylate) (D) and poly(propylene oxide) (P) were assembled as micelles into thin 150−250 nm thick films by LbL assembly with poly(acrylic acid) (PAA), including two D−P−D triblock copolymers, one having double the molecular weight of the other, and a D−P diblock copolymer. The BCP architectures strongly influenced the temperature-driven swelling of the mPEM thin films, with multilayers containing the triblock copolymers exhibiting better overall reversibility and stability than multilayers containing diblock copolymers.

2. MATERIALS AND METHODS

Materials. Poly(*N*,*N*-dimethylaminoethyl methacrylate-*b*-propylene oxide-*b*-*N*,*N*-dimethylaminoethyl methacrylate) (M_n: 1600-*b*-3000-*b*-1600, PI = 1.5) (STB), poly(propylene glycol) methyl ether (M_n = 3800 g/mol, PI = 1.12) (methoxy-P_{65}-OH), α,ω-dihydroxy-terminated poly(propylene oxide) (M_n = 7400 g/mol, PI = 1.07) (HO-P_{127}-OH), and poly(*N*,*N*-dimethylaminoethyl methacrylate) (M_n = 1300 g/mol, PI = 1.4) from Polymer Source; poly(acrylic acid) (M_w > 200 000 g/mol; 25% aqueous solution) (PAA) from Polysciences; triethylamine (TEA), 2-bromoisobutyryl bromide (BiBB), 2-(dimethylamino)ethyl methacrylate (98%) (DMA), copper(I) bromide (99.99%) (CuBr), 2,2′-bipyridyl (≥99%) (Bpy), 1,2-bis(2-iodoethoxy)ethane (BIEE), and 1,6-diphenyl-1,3,5-hexatriene (DPH) and all solvents (≥99.9%)—benzene, dichloromethane, methanol, hexane, and dimethylformamide—purchased from Aldrich were used as received unless otherwise mentioned.

Synthesis of Macroinitiators. Poly(propylene oxide) macroinitiators were prepared by esterification of the hydroxyl end groups of precursor molecules with BiBB. Commercially purchased (a) methoxy-P_{65}-OH (1.2 g, 29.3 mM) or (b) HO-P_{127}-OH (2.5 g, 27 mM) was dissolved in 100 mL of benzene. After removal of trace amounts of water by azeotropic distillation, the solution was cooled in an ice−water bath, and 2.5 mol equiv of TEA (73.3 mM for (a) or 135 mM for (b)) was added under vigorous stirring, followed by dropwise addition of BiBB (73.3 mM for (a) or 135 mM for (b)). The mixture was sealed and allowed to rise to room temperature overnight. At the end of the reaction, 1−2 drops of TEA was added and reacted with any excess BiBB for 1 h. The mixture was then filtered to remove amine salts, and the solvent was removed by distillation. The product was then dissolved in dichloromethane (DCM) and extracted 3 times with 5 wt % sodium bicarbonate solution. The final DCM layer was collected, dried over $MgSO_4$, and passed through a basic alumina column. The final methoxy-P_{65}-Br or difunctional Br-P_{127}-Br macroinitiators were then obtained by removal of DCM under vacuum.

Synthesis and Characterization of Diblock and Triblock Copolymers. The long triblock copolymer (LTB) and the diblock copolymer (DB) were synthesized by atomic transfer radical polymerization (ATRP) with a CuBr/Bpy catalytic system. The molar ratios of macroinitiator methoxy-P_{65}-Br:CuBr:Bpy:DMA was 1:1:2.5:60 for synthesis of DB, and that of Br-P_{127}-Br:CuBr:Bpy:DMA was 1:1:2.5:100 for synthesis of LTB. In brief, 1 g of macroinitiator was charged with DMA monomer (distilled under reduced pressure before use) and dissolved in ∼8 mL of methanol. The reaction mixture was degassed, and the CuBr/Bpy catalyst mixture was added under an argon atmosphere. The mixture was then degassed again, and polymerization was allowed to proceed at room temperature for 12 h under argon. The reaction was stopped by exposure to air. The products were purified by passage through a basic alumina column, removal of solvent under reduced pressure, and precipitation in cold hexane (−30 °C). The polymer products were dissolved in $CDCl_3$ for ^{1}H NMR characterization using a Bruker 400 MHz spectrometer and dissolved in dimethylformamide (DMF) for molecular weight and polydispersity determination by gel permeation chromatography (GPC) using PMMA calibration standards. DMF GPC measurements were obtained using a Water Breeze 1525 HPLC system operated at 75 °C.

BCP Solution Preparation and Characterization. To ensure solution equilibration, especially for the longest polymer LTB, all BCPs were dissolved at 1−2 mg/mL concentration in deionized, ultrapure Millipore water with resistivity 18 MΩ cm^{-3} (abbreviated as "DI" henceforth), acidified with 0.1 M HCl (0.5 mol equiv of the number of amine groups), by overnight refrigeration at 4 °C. The BCP solutions were then diluted to the desired concentration in room temperature DI water and adjusted to the desired pH by addition of 0.1 M NaOH or 0.1 M HCl. This solution was then refrigerated again for 5 h to allow for redissolution of polymers at the desired concentration and pH. After the solution was retrieved from the refrigerator and allowed (3−5 h) to equilibrate at room temperature, the pH was checked again and minor pH adjustments (if any) were made just prior to use of the solutions for microdifferential scanning calorimetry (mDSC), cryogenic scanning electron microscopy, shell cross-linking, dye solubilization, or LbL assembly. mDSC was done as described previously[30] to obtain the micellization temperature of 1 mg/mL BCP solutions at pH 8, and DPH dye solubilization, also described previously,[30] was carried out at room temperature on BCP solutions of concentrations between 0.0005 and 0.1 mg/mL for determination of BCP critical micelle concentration (CMC) at pH 7.

Cryogenic Scanning Electron Microscopy (Cryo-SEM). A FEI Helios 600 scanning electron microscope equipped with a Quorum Technologies PP2000 Cryo-SEM preparation system was used to obtain micelle images in the frozen state. BCP solutions of 0.1 mg/mL, pH 7, were injected into rivets glued end to end and inserted standing into holes in an aluminum holder such that the bottom rivet is held fixed while the top rivet stuck out above the holder. The solutions, mounted on a transfer device, were flash frozen in freshly melted liquid nitrogen slush (−210 °C) and transferred immediately under vacuum into a preparation vacuum chamber held at −130 °C. The top rivets were then knocked off to expose fracture surfaces within the interior region of the BCP solutions. Sublimation to expose BCP features was allowed to occur at −90 °C for 5 min, after which the temperature was reduced back to −130 °C and *in situ* sputtering of 1−2 nm of Au/Pd was carried out before SEM imaging of the surfaces at 5 kV and −190 °C.

Selective Cross-Linking of BCP Micelles. Cross-linking of DMA in the BCP micelle coronas was achieved at 25 °C and pH 7 by quaternization using BIEE, as described elsewhere.[39] Briefly, BIEE

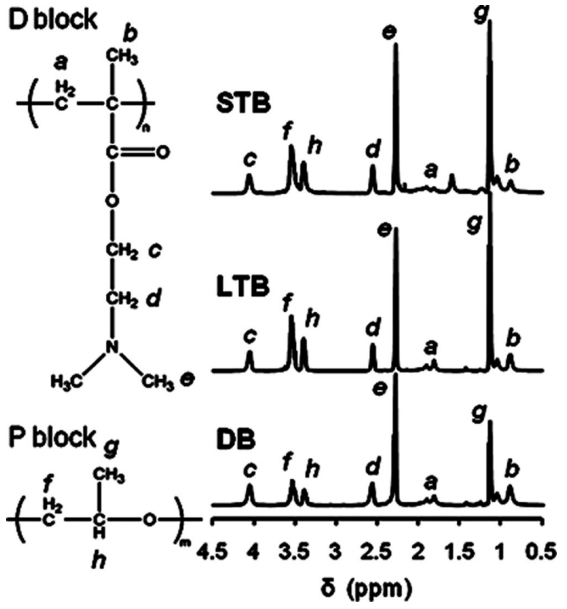

Figure 1. ^{1}H NMR spectra of the commercial short D−P−D triblock copolymer (STB) and synthesized block copolymers: long D−P−D triblock copolymer (LTB) and P−D diblock copolymer (DB) in $CDCl_3$.

(0.5 mol per mol of DMA residues) was added to 0.1 mg/mL BCP solutions adjusted to pH 7, and the reaction was allowed to proceed for 3 days.

LbL Assembly. BCP solutions at 0.1 mg/mL, pH 7, freshly constituted as described above were used for LbL assembly on silicon substrates prepared as detailed previously.[30] The 150−250 nm thick films were assembled for temperature dependent swelling studies. The films are denoted by $(\text{polycation/polyanion})_x$ where the polycation is poly(*N*,*N*-dimethylaminoethyl methacrylate) (D) or positively charged BCP micelles of STB, LTB, or DB and the polyanion is PAA. The subscript x denotes the number of polycation−polyanion deposition cycles. The 150−250 nm thick films studied correspond to $(\text{STB/PAA})_{30}$, $(\text{LTB/PAA})_{35}$, $(\text{DB/PAA})_{35}$, and $(\text{D/PAA})_{40}$. The subscripts are dropped for simplicity in the Results and Discussion section. All multilayers were deposited on 1 mm thick silicon wafers with both polymer solutions and rinse solutions adjusted to pH 7 with 1 M HCl and 1 M NaOH.

Spectroscopic Ellipsometry. The dry film thicknesses and swelling behavior of the films in pH 7 DI were determined using a Woollam VASE spectroscopic ellipsometer, as described in detail previously.[30] In order to hold the films at low temperature in pH 7 DI for time dependent swelling studies, the fluid cell used for *in situ* ellipsometry was housed in a custom-made hollow stainless steel block through which cold water was circulated using a Julabo refrigerated circulator with PID1 temperature control, able to provide temperature stability of 0.03 °C.

Atomic Force Microscopy (AFM). All AFM images were obtained using a Digital Instruments Nanoscope IV, Dimension 3000 microscope operated in tapping mode. FM-20 AFM probes from NanoWorld with force constant 2.8 N/m, resonant frequency 75 kHz, and tip radius less than 8 nm were used for imaging.

3. RESULTS AND DISCUSSION

3.1. BCP Synthesis and Characterization. As described in the Materials and Methods, macroinitiators of poly(propylene oxide) (P) with either one or both ends functionalized with Br were used to initiate ATRP of DMA monomers for synthesis of the P−D diblock copolymer (DB) or the D−P−D long triblock copolymer (LTB), respectively. ^{1}H NMR spectroscopy in $CDCl_3$ was used to determine the degree of polymerization of the D blocks grown from the P block macroinitiators of known molecular weight. Figure 1 shows the ^{1}H NMR spectra of the synthesized block copolymers LTB and DB along with the spectrum of the commercial D−P−D short triblock copolymer (STB).

From integration of the nonoverlapping peaks from the 2 ($-CH_2-$N) protons of the D block at δ = 4.06 (denoted *c* in Figure 1) and integration of the peaks at δ = 3.54 and 3.40

Table 1. Composition and Polydispersity of Block Copolymers

polymer	D:P[a]	N_P[b,e]	N_D[c]	block architecture	M_w/M_n
STB	0.41	52	22	$D_{11}-P_{52}-D_{11}$	1.5[e]
LTB	0.41	127	54	$D_{27}-P_{127}-D_{27}$	1.38[d]
DB	0.88	65	57	$D_{57}-P_{65}$	1.66[d]

[a] Ratio of D to P units determined by ^{1}H NMR spectroscopy in $CDCl_3$. [b] Degree of polymerization of P. [c] Degree of polymerization of D. [d] Polydispersity of synthesized BCPs determined by GPC in DMF using poly(methyl methacrylate) calibration standards. [e] Information provided by Polymer Source Inc. from which macroinitiators and STB were purchased.

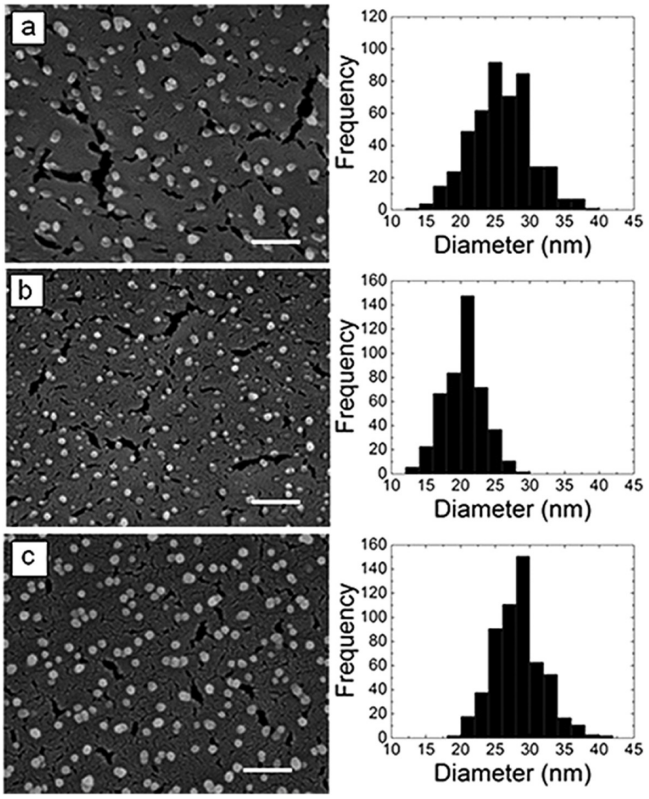

Figure 2. Cryo-SEM images of freeze fractured surfaces of flash-frozen BCP solutions, taken after sublimation to expose micelles. STB (a), LTB (b), and DB (c) solutions were of 0.1 mg/mL concentration in DI water, adjusted to pH 7. The white scale bars at the bottom right of each image represent 150 nm. Size distributions of micelles obtained by measurements from at least four images are shown on the right-hand side of each representative image.

Table 2. BCP Solution Micellization Characteristics

polymer	micelle diameter[a] (nm)	MT[b] (°C)	CMC[c] (mg/mL)
STB	26 ± 5	16	0.05
LTB	21 ± 3	10	0.02
DB	28 ± 3	15	0.04

[a] Average BCP micelle size and standard deviation of measurements obtained from cryo-SEM images of 0.1 mg/mL BCP solutions at pH 7, 22 °C. [b] Micellization temperature (MT) of 1 mg/mL BCP solutions adjusted to pH 8, determined using micro-differential scanning calorimetry. [c] Critical micelle concentration (CMC) at 22 °C, pH 7, determined by DPH dye solubilization.

corresponding to 3 protons (−O−CH_2−CH−) (*f* and *h*) along the polymer backbone of P, the compositions of the BCPs were determined as listed in Table 1. Gel permeation chromatography (GPC) in dimethylformamide (DMF) solvent was carried out on the macroinitiators and the synthesized BCP products to determine the polydispersity of the polymers. GPC curves are shown in the Supporting Information (Figure S1), and the polydispersities (M_w/M_n) of the block copolymers are listed in Table 1.

3.2. BCP Solution Self-Assembly. To determine the aggregate morphology of the BCPs present in the solutions used for LbL deposition, we used cryogenic scanning electron microscopy (cryo-SEM). Solutions of each BCP were prepared at 0.1 mg/mL in DI water and adjusted to pH 7, identical to conditions used for LbL assembly. The solutions were vitrified in liquid nitrogen slush to avoid ice crystal formation and fractured at −130 °C to expose the internal structure of the frozen solution. To enhance the topography, these exposed surfaces were held at low pressure (10^{-4} Pa) and −90 °C to remove water by sublimation, leaving behind the BCP structures. Figure 2 shows that all three BCPs exist as relatively monodisperse spherical micelles in solution under the LbL assembly conditions. Analysis of several cryo-SEM images allowed us to determine the diameters of micelles and histograms of the micelle size distribution are shown to the right of the representative SEM images. The average micelle diameters of the BCPs along with the standard deviation of the measurements are listed in Table 2. The sizes reported here are likely to be smaller than the hydrated micelle size due to removal of water by sublimation. Nonetheless, it is interesting to note that the differences in molecular weight and block architecture between the BCPs did not have a significant effect on the observed micelle sizes. This is possible because while the micelle core radius and aggregation number tend to increase with the core forming P block length,[40,41] increasing the corona block length is expected to cause an opposite trend and a decrease in aggregation number.[40−42] It is useful to note that in cryo-SEM optimizing the sublimation step (through time and temperature control) is important. While sufficient sublimation is needed to allow exposure of micelles at the surface, too much sublimation exposes several layers of micelles. In the latter case, large aggregates are seen, which upon close inspection can be discerned to be clusters of smaller spherical micelles piled up on one another (shown in Figure S3). Solutions of higher BCP concentrations 1 up to 5 mg/mL were prepared and imaged under the same conditions. Large hollow tubes, discs, reticulated networks, and sheet-type BCP structures were readily observed at the higher concentrations (data not shown), providing reassurance that the simple spherical micelle was the dominant BCP structure in the 0.1 mg/mL solutions used for LbL assembly.

The solution micellization temperatures (MTs) of 1 mg/mL BCP solutions were determined using micro-differential scanning calorimetry (mDSC), as detailed in our previous work.[30] The MTs are listed in Table 2. Since micellization temperature is sensitive to the solution pH,[30] the MT was determined at pH 8 to avoid possible suppression of micellization by highly charged D blocks.[30,41,43−45] While solutions of a different pH and concentration were used for mDSC due to sensitivity limitations, the trend in MT determined at pH 8, 1 mg/mL BCP solutions and the absolute values of MTs corresponded well to the temperature at which aggregation was detected by DLS in solutions at pH 7, 0.1 mg/mL (Figure S2). The CMC of the BCPs at room temperature (22 °C) was determined using a well-established DPH dye solubilization technique.[46] Here, BCP solutions of concentrations 0.0005, 0.001, 0.01, 0.02, 0.04, 0.06, 0.08, and 0.1 mg/mL were made, adjusted to pH 7, redissolved at low temperature, and allowed to equilibrate at room temperature for 5 h, after which DPH was added and allowed to equilibrate in the BCP solution for another 5 h. The fluorescence spectra of these solutions were then obtained, and the fluorescence intensity at 457 nm was plotted as a function of BCP concentration (Figure S4). The CMC values listed in Table 2 were determined as the point at which a steep increase in fluorescence intensity with increasing polymer concentration was observed.

As seen in Table 2, both the micellization temperature and critical micelle concentration of the BCPs decreased with the molecular weight of the poly(propylene oxide) (P) block. The decrease in micellization temperature at fixed concentration logically follows from the expected decrease of lower critical solution temperature (LCST) with molecular weight. The CMC at 22 °C also decreases in the order of P block length. While the longer poly(*N*,*N*-dimethylaminoethyl methacrylate) (D) end block could be expected to contribute to an opposite trend, where longer D blocks would tend to lower the CMC and CMT, the effects of the P block length dominate in this case. Similar decreases in CMC and CMT with P block molecular weight have been reported for Pluronics, that is, di- and triblock copolymers of poly(propylene oxide) and poly(ethylene oxide) blocks instead of D blocks.[46]

As detailed in our previous work,[30] the assembly pH and anionic binding partner used for LbL assembly of temperature responsive D−P−D triblock copolymers are key factors that determine whether the final films are able to respond to changes in temperature with large changes in swelling degree. There we found that using a strong polyacid, poly(4-styrenesulfonate), as the anionic binding partner prohibited large swelling transitions. When a weak polyacid, poly(acrylic acid) (PAA), was used for the assembly, large reversible swelling transitions were observable for systems deposited at pH 7 but not at pH 4. On the basis of those findings, we assemble thin films from micelle containing BCP solutions of STB, LTB, or DB with PAA at pH 7 to expose the effects of block copolymer architecture on the temperature triggered swelling responses of mPEMs. It is important to note that the P−D−P triblock copolymer used in our previous study,[30] though of the same average composition as STB used in this work, differs in terms of polydispersity. In the previous study, the P−D−P block copolymer had end blocks of broad polydispersity, while here STB has a polydispersity of 1.5 for meaningful comparison with the other two block copolymer architectures. Since all multilayers were assembled at pH 7, the nomenclature for the mPEMs in the following discussions is simplified just to contain the component polymer pairs. The temperature dependent swelling responses of (STB/PAA), (LTB/PAA), and (DB/PAA) mPEMs of comparable thicknesses between 150 and 250 nm were investigated.

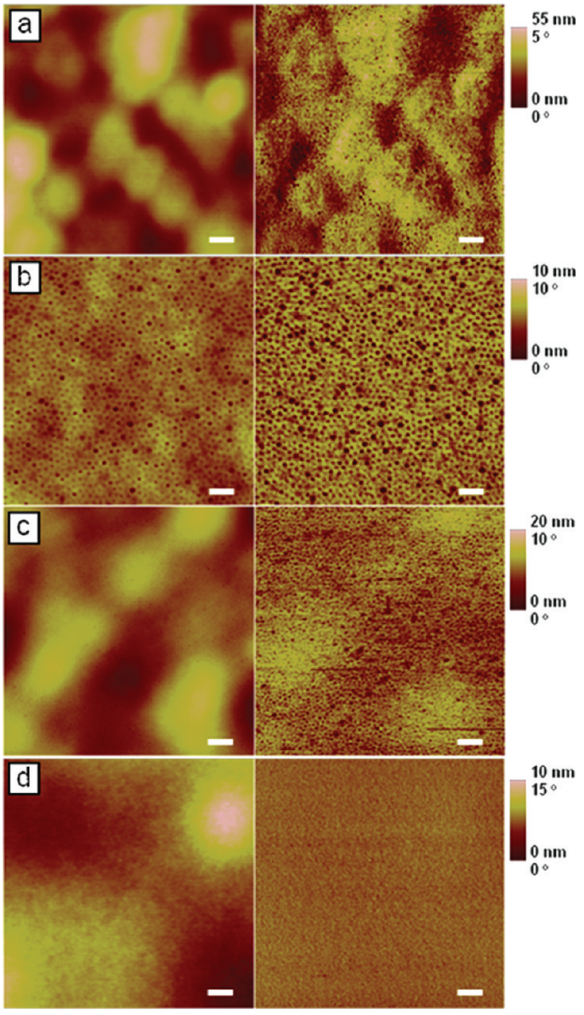

Figure 3. 1 μm × 1 μm atomic force microscope (AFM) images of BCP or homopolymer, poly(*N*,*N*-dimethylaminoethyl methacrylate) (D), multilayers assembled with PAA. The left column consists of height images while the right column consists of phase images. Rows a, b, c, and d correspond to multilayers of $(STB/PAA)_{30}$, $(DB/PAA)_{35}$, $(LTB/PAA)_{35}$, and control $(D/PAA)_{40}$, respectively. White scale bars on images represent 100 nm, while height and phase scales are shown on the right.

3.3. Surface Morphology of BCP Micelle LbL Assemblies.

As seen from AFM images of dried micelle polyelectrolyte multilayers (mPEMs) in Figure 3, the multilayers made with the shorter BCPs (STB and DB) are significantly rougher than the mPEM made from the higher molecular weight LTB. The rms roughness values obtained from the images of the (STB/PAA), (DB/PAA), (LTB/PAA), and (D/PAA) multilayers are 10, 4, 1, and 2 nm, respectively. Unlike spherical structures expected for BCP micelle containing multilayers, as previously reported by several groups,[22,23,31,34] we observed surface depressions (described as "dimples" henceforth) that are especially well ordered in the case of (LTB/PAA).

The dimpled surface morphologies seen in the mPEMs are absent in the control assembly of D homopolymer with PAA assembled at the same pH of 7. Dimples seen in all mPEMs have regular lateral dimensions on the order of 10−30 nm, and most have depths of less than 2 nm, with the exception of the more prominent dimples seen in (LTB/PAA) that have depths up to

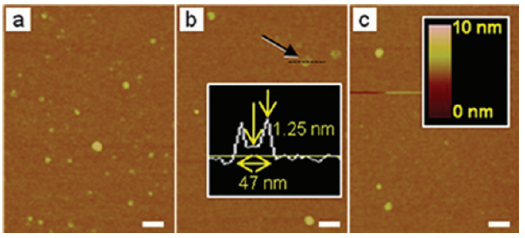

Figure 4. AFM images of BIEE shell cross-linked BCPs: STB (a), LTB (b), and DB (c), dip-coated onto the surface of silicon wafers. The inset in (b) shows the height profile along the dotted line. All images have the same lateral and height scales. The height scale is shown as an inset in (c), and scale bars on the bottom right corners represent 100 nm.

6 nm. Since these types of surface morphologies had not been reported for BCP micelle multilayers before, we seek to clarify the origins of these surface structures, which, at a glance, resemble cavitated micelles[47] or toroid[48,49] type morphologies. To investigate this, we carried out solution cross-linking of micelles to determine what surface adsorbed BCPs would look like if surface rearrangement and micelle dissolution could be prevented through cross-linking. 1,2-Bis(2-iodoethoxy)ethane (BIEE) was used to cross-link D blocks in the micelle corona through quaternization of the tertiary amine groups. This cross-linking technique has frequently been applied to stabilize D block containing BCP micelles, and several publications, particularly by the Armes group, describe this chemistry in detail.[50−52] In this work, we used the protocol of Jiang et al.[39] at room temperature to selectively cross-link the coronas of our BCPs at 0.1 mg/mL, pH 7. Cross-linking was allowed to proceed for 3 days, after which the cross-linked BCP micelles were dip-coated onto silicon wafers, allowed to dry, and imaged with AFM in the dry state. By cross-linking the D end blocks in the corona of the micelles in solution, the spherical shapes of micelles were better preserved, and circular disks can be observed on the dip-coated silicon water, as seen in Figure 4a. Despite corona cross-linking, spreading and flattening of the cross-linked micelles on the silicon surface were observable, with the circular disklike structures having diameters of 40−60 nm, several times greater than their corresponding heights of 3−6 nm (Figure 4a−c). This indicated significant chain mobility, even within corona cross-linked micelles, that allowed for changes in micelle shape upon surface attachment. Several structures that resemble the dimpled surface structures on mPEMs were also observed, as pointed out by the arrow in Figure 4b. As shown in the line section height profile (inset of Figure 4b), these features, unlike toroids, are not hollow in the central region but, rather, are disks with raised edges. While these structures could result from micelle cores that are not fully dehydrated, this is unlikely the case with several reports suggesting that micelle cores formed by P blocks are anhydrous and dense.[53−55] Without core plasticization by water molecules, significant surface rearrangement is still possible due to the low glass transition temperature ($T_g \sim -75$ °C[56,57]) of the poly(propylene oxide) core. The depth profiles (like the inset in Figure 4b) of dimple-type structures observed in multiple images of corona cross-linked micelles show that the central depression is typically 1−2 nm deep. This depth agrees well with the depths of dimples observed on the surface of the dry multilayers, showing that these structures in mPEMs originate directly from the BCP micellar self-assembly in solution and not as a consequece of the LbL process with PAA. The well-ordered surface

dx.doi.org/10.1021/ma201397d |*Macromolecules* 2011, 44, 7767–7774

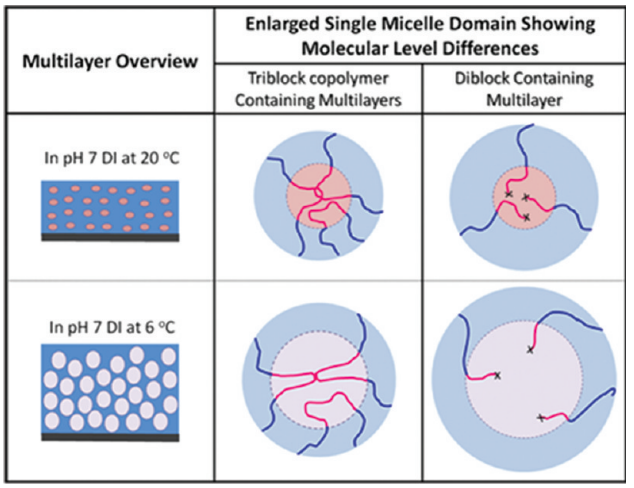

Figure 5. Drawings depicting the molecular configurations of BCPs within the mPEMs studied. The blue region surrounding the micelle cores are composed of D corona blocks ionically cross-linked to PAA chains (PAA not drawn for simplicity). The top row represents the multilayers in pH 7 DI water at 20 °C where the P domains are poorly hydrated, while the bottom row represents the multilayers at 6 °C where micelle cores of all BCPs become highly swollen with water.

patterns that can be achieved using LbL assembly of LTB micelles offers patterned surface heterogeneity on a 15−30 nm length scale. Ordering is less pronounced in the AFM images of the shorter (STB/PAA) and (DB/PAA) multilayers and could be related to AFM imaging resolution limitations.

3.4. Thin Film mPEM Temperature Swelling Responses in Water. We examined the temperature responsive swelling properties of our mPEM thin films. The three BCPs studied contain the same temperature responsive block, P, while differing in overall molecular weight and connectivity. At the supramolecular level (depicted in the leftmost column of Figure 5), the domain sizes and size distribution of the temperature responsive P micelle cores within all three BCP containing multilayers are expected to look relatively similar based on the solution, surface adsorption, and dry state AFM studies described above. We expect the cross section of the multilayer films to be comprised of P block domains of micelle cores (pink dots) surrounded (in blue) by micelle coronas of D blocks that are associated with PAA through ionic interactions between the protonated tertiary amine groups on the D block and ionized carboxylic acid groups on PAA. In DI water at room temperature, the P blocks are poorly hydrated and preferentially self-aggregate in the micellar cores.[53−55] When the temperature is decreased to 6 °C, hydrogen bonding enhances water's interaction with the P blocks, causing the P block domains to swell.[53−55] It is at these lower temperatures that differences in molecular connectivity between the triblock and diblock copolymers can become important, as shown schematically in the bottom row of Figure 5.

As reported in our previous study, D−P−D triblock copolymers assembled with PAA at pH 7 exhibit temperature-driven, reversible, swelling transitions.[30] In that work, only the instantaneous swelling response was accessible by *in situ* ellipsometric determination of wet film thickness upon addition of precooled aqueous solutions. With an improved setup (details in Materials and Methods section), we were able to investigate film swelling as a function of time while the mPEMs were immersed in pH 7 adjusted DI water at a controlled low temperature. As seen in

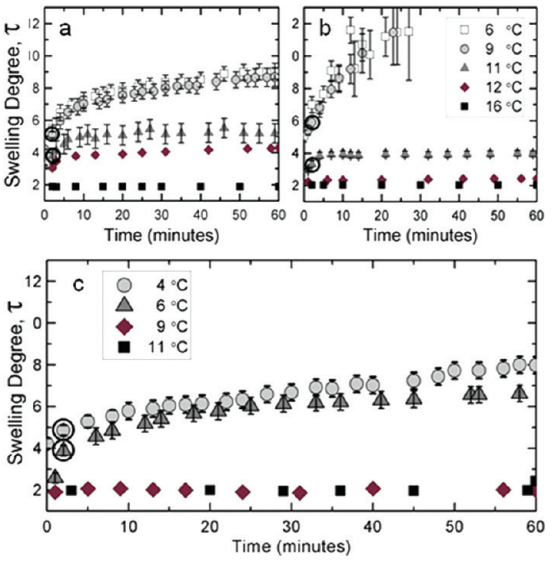

Figure 6. Graphs showing the time-dependent evolution of the swelling degree (τ = wet film thickness/dry film thickness) of mPEMs, (a) (STB/PAA), (b) (DB/PAA), and (c) (LTB/PAA) held at various temperatures. All films studied were of similar thicknesses between 150 and 250 nm. The swelling degrees at 2 min of low temperature exposure are circled as they correspond to points subsequently discussed in Figure 8.

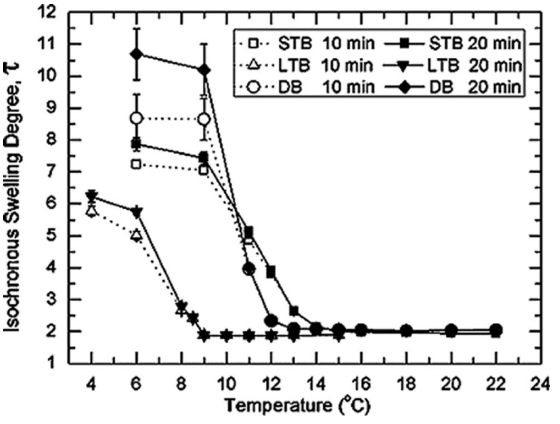

Figure 7. Isochronous swelling degree, τ = wet thickness/dry thickness, of mPEM films held at various temperatures for 10 min (hollow symbols with dotted lines) or 20 min (solid symbols and lines). Legend indicates the BCP component of the mPEMs for convenient identification of curves.

Figure 6, the degree of swelling, τ = wet film thickness/dry film thickness, shows both time and temperature dependence. Notably, the isochronous degree of swelling increases with decreasing temperature and the time dependence of swelling becomes more significant at lower temperatures.

As seen in Figure 6, increased swelling with low-temperature exposure, if any, is measurable within 2 min. To determine the mPEM film swelling transition temperature (T_{stt}), below which increased film swelling occurs, isochronous values of τ at 10 and 20 min are plotted as a function of temperature in Figure 7. The curves show distinct swelling transitions near 13.5, 12, and 8.5 °C for the STB, DB, and LTB containing mPEMs, respectively. At small degrees of undercooling, equilibrium can be established where the mixing and elastic contributions to free energy balance

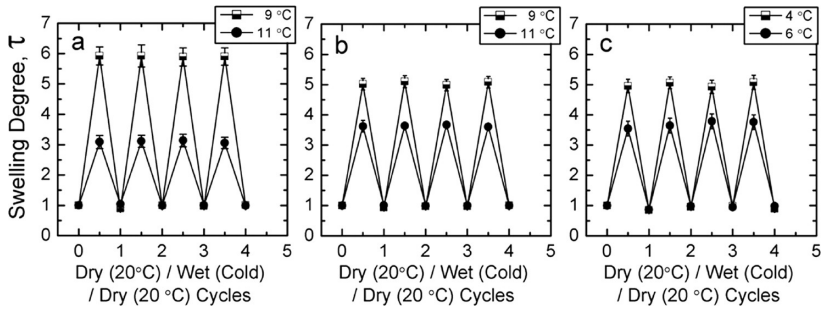

Figure 8. Changes in swelling degree, τ, of mPEMs: (a) (DB/PAA), (b) (STB/PAA), and (c) (LTB/PAA), upon cycling between the dry state at room temperature (20 °C), wet state in cold DI water adjusted to pH 7 at 2 min immersion times, and deswollen and dried at (20 °C).

out and steady-state swelling can be achieved (as seen in Figure 6a at 11 and 12 °C, Figure 6b at 11 °C, and Figure 6c at 6 °C). With greater undercooling, the increasingly favored solvent-polymer interactions result in swelling forces strong enough to cause creep behavior and the degree of swelling increases with time as seen at lower temperatures in Figure 6. The transition between time-independent and time-dependent swelling is clear in Figure 7 where the 10 and 20 min curves deviate at a certain degree of cooling below T_{stt}. It is in this low-temperature, time-dependent swelling regime that differences between the triblock and diblock containing films become significant. Comparing the dynamic swelling curves in the low-temperature range in Figure 6, we see that while (DB/PAA) quickly swells to failure at 9 °C, both (STB/PAA) and (LTB/PAA) are able to sustain stable τ values in the range of 4−10. Deswelling and drying of the triblock based mPEMs from any of the points in Figure 6 revealed no film loss, whereas diblock containing films swollen at 6 or 9 °C showed significant (60−80%) film loss when exposed to these temperatures for more than 30 min. As illustrated in Figure 5, the mPEMs that contain triblock copolymers, (STB/PAA) and (LTB/PAA), have connectivity in the P domains, in turn covalently linked to D blocks in the ionically stabilized network. This topological connectivity in the triblocks leads to equilibrium load-bearing trapped entanglements that are not present in the diblock system. Consequently, the diblock-containing mPEMs show the largest propensity to disintegrate at low temperatures, whereas the triblock-containing systems show greater ability to sustain controlled swelling and exhibit a greater range of reversible swelling phenomena.

Despite the time-dependent creep observed during extended low-temperature exposure, Figure 8 shows that the short-time swelling response (points circled in Figure 6) is reproducible and essentially fully reversible for all the BCP systems studied; no film lost or history dependence of this short time response was detected with repeated swelling and deswelling cycles. The degree of swelling recorded at 2 min of low temperature exposure increased with the degree of undercooling, $\Delta T = T - T_{stt}$. In Figure 8, the reversible short time swelling response at $\Delta T = 4$ or 6 °C is presented. These undercooling values correspond to temperatures of ∼11 and 9 °C for the STB and DB multilayers and 6 or 4 °C for the LTB multilayer. The degree of swelling, τ, being a function of temperature and swelling time, is denoted as $\tau_x(\Delta T,t)$, where x is the BCP component present in the film under consideration, ΔT is the undercooling in °C, and t is the swelling time in minutes. From Figure 8b,c, we see that the short time swelling response of the triblock copolymers with different molecular weights but the same P:D ratios is similar to $\tau_{STB}(4,2) \approx \tau_{LTB}(4,2) \approx 3.6$ and $\tau_{STB}(6,2) \approx \tau_{LTB}(6,2) \approx 5$. In this respect, the overall triblock molecular weight did not affect the reversible behavior. In this short time regime, however, the diblock-containing mPEM films (Figure 8a) show marked differences from their triblock counterparts (Figure 8b,c), swelling to lower extents than the triblock containing films at ΔT = 4 °C and to greater extents at ΔT = 6 °C. The lower degree of swelling at ΔT = 4 °C could reflect the lower P:D ratio of DB while the higher degree of swelling at ΔT = 6 °C is likely the effect of connectivity differences discussed above.

4. CONCLUSIONS

In this paper, we have exposed the effects of BCP architecture on the properties of temperature responsive mPEM thin films created by the LbL assembly. We found that both the solution micellization temperature (MT) and film swelling transition temperature (T_{stt}) depend on P block length. Importantly, our results reveal that while all three BCPs can be used to create temperature responsive films, the range of accessible reversible swelling depends critically on BCP connectivity. While the diblock containing films quickly swell to the point of failure at ΔT = 6 or more, the triblock copolymer containing multilayers, both (STB/PAA) and (LTB/PAA), are able to sustain significantly lower rates of creep and sustained swollen states with prolonged low-temperature exposure. The differences in dynamic swelling responses uncovered in this study have significant implications in the application of these temperature-swellable films. Where they might be suited for applications that require repeated rapid and transient low temperature exposure, the diblock copolymer containing films cannot be exposed to low temperature for long. In contrast, the disintegration of the diblock copolymer containing film at low temperature could make it useful as a low temperature release system. In addition, the understanding gained in this study suggests that star block copolymers with covalently connected temperature responsive core blocks and polyelectrolyte end blocks will be ideal architectures for the creation of creep-resistant temperature-swellable multilayers.

■ ASSOCIATED CONTENT

Supporting Information. (1) Gel permeation chromatography curves of poly(propylene oxide) macroinitiators and block copolymers, (2) dynamic light scattering data, (3) additional cryogenic scanning electron microscopy images, and (4) fluorescence data for determination of the CMC. This material is available free of charge via the Internet at http://pubs.acs.org.

AUTHOR INFORMATION

Corresponding Author
*E-mail: rubner@mit.edu (M.F.R.); recohen@mit.edu (R.E.C.).

ACKNOWLEDGMENT

This work was supported by the MRSEC Program of the National Science Foundation under award DMR-0819762 and in part by NSF DMR-0906474 (S.A.S.) and the Agency for Science Technology and Research (A*STAR), Singapore, through funding of W.S.T. under the NSS(pHD) National Science Scholarship. We thank the Center for Materials Science and Engineering (CMSE), the Institute for Soldier Nanotechnologies (ISN), and Prof. T. Alan Hatton for use of their characterization facilities.

REFERENCES

(1) Westman, L.; Lindström, T. *J. Appl. Polym. Sci.* **1981**, *26*, 2533.
(2) Skouri, R.; Schosseler, F.; Munch, J. P.; Candau, S. J. *Macromolecules* **1995**, *28*, 197.
(3) Raj Singh, T. R.; Woolfson, A. D.; Donnelly, R. F. *J. Pharm. Pharmacol.* **2010**, *62*, 829.
(4) Kanazawa, H. *J. Sep. Sci.* **2007**, *30*, 1646.
(5) Nagase, K.; Kobayashi, J.; Kikuchi, A.; Akiyama, Y.; Kanazawa, H.; Okano, T. *Biomaterials* **2011**, *32*, 619.
(6) Peppas, N. A.; Khare, A. R. *Adv. Drug Delivery Rev.* **1993**, *11*, 1.
(7) Dadsetan, M.; Liu, Z.; Pumberger, M.; Giraldo, C. V.; Ruesink, T.; Lu, L.; Yaszemski, M. J. *Biomaterials* **2010**, *31*, 8051.
(8) Dong, L.; Jiang, H. *Soft Matter* **2007**, *3*, 1223.
(9) Gerlach, G.; Guenther, M.; Sorber, J.; Suchaneck, G.; Arndt, K.-F.; Richter, A. *Sens. Actuators, B* **2005**, *111*−*112*, 555.
(10) Discher, D. E.; Janmey, P.; Wang, Y.-l. *Science* **2005**, *310*, 1139.
(11) Wong, J. Y.; Velasco, A.; Rajagopalan, P.; Pham, Q. *Langmuir* **2003**, *19*, 1908.
(12) Lichter, J. A.; Thompson, M. T.; Delgadillo, M.; Nishikawa, T.; Rubner, M. F.; Van Vliet, K. J. *Biomacromolecules* **2008**, *9*, 1571.
(13) Itano, K.; Choi, J.; Rubner, M. F. *Macromolecules* **2005**, *38*, 3450.
(14) Hiller, J. A.; Rubner, M. F. *Macromolecules* **2003**, *36*, 4078.
(15) Déjugnat, C.; Sukhorukov, G. B. *Langmuir* **2004**, *20*, 7265.
(16) Kozlovskaya, V.; Kharlampieva, E.; Mansfield, M. L.; Sukhishvili, S. A. *Chem. Mater.* **2005**, *18*, 328.
(17) Lee, D.; Nolte, A. J.; Kunz, A. L.; Rubner, M. F.; Cohen, R. E. *J. Am. Chem. Soc.* **2006**, *128*, 8521.
(18) Kim, B.-S.; Lee, H.-i.; Min, Y.; Poon, Z.; Hammond, P. T. *Chem. Commun.* **2009**, 4194.
(19) Kharlampieva, E.; Kozlovskaya, V.; Tyutina, J.; Sukhishvili, S. A. *Macromolecules* **2005**, *38*, 10523.
(20) Glinel, K.; Déjugnat, C.; Prevot, M.; Schöler, B.; Schönhoff, M.; Klitzing, R. v. *Colloids Surf., A* **2007**, *303*, 3.
(21) Quinn, J. F.; Caruso, F. *Langmuir* **2003**, *20*, 20.
(22) Zhu, Z.; Sukhishvili, S. A. *ACS Nano* **2009**, *3*, 3595.
(23) Xu, L.; Zhu, Z.; Sukhishvili, S. A. *Langmuir* **2010**, *27*, 409.
(24) Nolan, C. M.; Serpe, M. J.; Lyon, L. A. *Biomacromolecules* **2004**, *5*, 1940.
(25) Zhuk, A.; Pavlukhina, S.; Sukhishvili, S. A. *Langmuir* **2009**, *25*, 14025.
(26) Gui, Z.; Qian, J.; Zhao, Q.; Ji, Y.; Liu, Y.; Liu, T.; An, Q. *Colloids Surf., A* **2011**, *380*, 270.
(27) Steitz, R.; Leiner, V.; Tauer, K.; Khrenov, V.; v. Klitzing, R. *Appl. Phys. A: Mater. Sci. Process.* **2002**, *74*, s519.
(28) Glinel, K.; Sukhorukov, G. B.; Möhwald, H.; Khrenov, V.; Tauer, K. *Macromol. Chem. Phys.* **2003**, *204*, 1784.
(29) Jaber, J. A.; Schlenoff, J. B. *Macromolecules* **2005**, *38*, 1300.
(30) Tan, W. S.; Cohen, R. E.; Rubner, M. F.; Sukhishvili, S. A. *Macromolecules* **2010**, *43*, 1950.
(31) Cho, J.; Hong, J.; Char, K.; Caruso, F. *J. Am. Chem. Soc.* **2006**, *128*, 9935.
(32) Hong, J.; Bae, W. K.; Lee, H.; Oh, S.; Char, K.; Caruso, F.; Cho, J. *Adv. Mater.* **2007**, *19*, 4364.
(33) Qi, B.; Tong, X.; Zhao, Y. *Macromolecules* **2006**, *39*, 5714.
(34) Ma, N.; Wang, Y.; Wang, Z.; Zhang, X. *Langmuir* **2006**, *22*, 3906.
(35) Addison, T.; Cayre, O. J.; Biggs, S.; Armes, S. P.; York, D. *Langmuir* **2008**, *24*, 13328.
(36) Kim, B.-S.; Park, S. W.; Hammond, P. T. *ACS Nano* **2008**, *2*, 386.
(37) Nguyen, P. M.; Zacharia, N. S.; Verploegen, E.; Hammond, P. T. *Chem. Mater.* **2007**, *19*, 5524.
(38) Lin, J.; Zhu, J.; Chen, T.; Lin, S.; Cai, C.; Zhang, L.; Zhuang, Y.; Wang, X.-S. *Biomaterials* **2009**, *30*, 108.
(39) Jiang, X.; Ge, Z.; Xu, J.; Liu, H.; Liu, S. *Biomacromolecules* **2007**, *8*, 3184.
(40) Nagarajan, R.; Ganesh, K. *Macromolecules* **1989**, *22*, 4312.
(41) Zhulina, E. B.; Borisov, O. V. *Macromolecules* **2002**, *35*, 9191.
(42) Shusharina, N. P.; Linse, P.; Khokhlov, A. R. *Macromolecules* **2000**, *33*, 8488.
(43) Xu, L.; Zhu, Z.; Borisov, O. V.; Zhulina, E. B.; Sukhishvili, S. A. *Phys. Rev. Lett.* **2009**, *103*, 118301.
(44) Lee, A. S.; Bütün, V.; Vamvakaki, M.; Armes, S. P.; Pople, J. A.; Gast, A. P. *Macromolecules* **2002**, *35*, 8540.
(45) Lee, A. S.; Gast, A. P.; Bütün, V.; Armes, S. P. *Macromolecules* **1999**, *32*, 4302.
(46) Alexandridis, P.; Holzwarth, J. F.; Hatton, T. A. *Macromolecules* **1994**, *27*, 2414.
(47) Boontongkong, Y.; Cohen, R. E. *Macromolecules* **2002**, *35*, 3647.
(48) O'Driscoll, S. M.; O'Mahony, C. T.; Farrell, R. A.; Fitzgerald, T. G.; Holmes, J. D.; Morris, M. A. *Chem. Phys. Lett.* **2009**, *476*, 65.
(49) Huang, H.; Chung, B.; Jung, J.; Park, H.-W.; Chang, T. *Angew. Chem., Int. Ed.* **2009**, *48*, 4594.
(50) Bütün, V.; Lowe, A. B.; Billingham, N. C.; Armes, S. P. *J. Am. Chem. Soc.* **1999**, *121*, 4288.
(51) Liu, S.; Weaver, J. V. M.; Tang, Y.; Billingham, N. C.; Armes, S. P.; Tribe, K. *Macromolecules* **2002**, *35*, 6121.
(52) Li, Y.; Du, J.; Armes, S. P. *Macromol. Rapid Commun.* **2009**, *30*, 464.
(53) Alexandridis, P.; Nivaggioli, T.; Hatton, T. A. *Langmuir* **1995**, *11*, 1468.
(54) Guo, C.; Liu, H. Z.; Chen, J. Y. *Colloid Polym. Sci.* **1999**, *277*, 376.
(55) Cau, F.; Lacelle, S. *Macromolecules* **1996**, *29*, 170.
(56) Johari, G. P. *Polymer* **1986**, *27*, 866.
(57) Allen, G.; Booth, C.; Jones, M. N.; Marks, D. J.; Taylor, W. D. *Polymer* **1964**, *5*, 547.